energies

MDPI

Article

Thermoelectric Properties of Alumina-Doped $Bi_{0.4}Sb_{1.6}Te_3$ Nanocomposites Prepared through Mechanical Alloying and Vacuum Hot Pressing

Chung-Kwei Lin [1], May-Show Chen [2,3], Rong-Tan Huang [4], Yu-Chun Cheng [4] and Pee-Yew Lee [4,*]

Received: 20 July 2015 ; Accepted: 23 October 2015 ; Published: 6 November 2015
Academic Editor: Shi Xue Dou

1 School of Dental Technology, College of Oral Medicine, Taipei Medical University, Taipei 110, Taiwan; chungkwei@tmu.edu.tw
2 School of Oral Hygiene, College of Oral Medicine, Taipei Medical University, Taipei 110, Taiwan; maychen@tmu.edu.tw
3 Department of Dentistry, Taipei Medical University Hospital, Taipei 110, Taiwan
4 Institute of Materials Engineering, National Taiwan Ocean University, Keelung 202, Taiwan; rthuang@ntou.edu.tw (R.H.); yuchuncheng1@gmail.com (Y.C.)
* Correspondence: pylee@ntou.edu.tw; Tel.: +886-2-2469-3078; Fax: +886-2-2462-5324

Abstract: In this study, γ-Al_2O_3 particles were dispersed in *p*-type $Bi_{0.4}Sb_{1.6}Te_3$ through mechanical alloying to form γ-Al_2O_3/$Bi_{0.4}Sb_{1.6}Te_3$ composite powders. The composite powders were consolidated using vacuum hot pressing to produce nano- and microstructured composites. Thermoelectric (TE) measurements indicated that adding an optimal amount of γ-Al_2O_3 nanoparticles improves the TE performance of the fabricated composites. High TE performances with figure of merit (ZT) values as high as 1.22 and 1.21 were achieved at 373 and 398 K for samples containing 1 and 3 wt % γ-Al_2O_3 nanoparticles, respectively. These ZT values are higher than those of monolithic $Bi_{0.4}Sb_{1.6}Te_3$ samples. The ZT values of the fabricated samples at 298–423 K are 1.0–1.22; these ZT characteristics make γ-Al_2O_3/$Bi_{0.4}Sb_{1.6}Te_3$ composites suitable for power generation applications because no other material with a similarly high ZT value has been reported at this temperature range. The achieved high ZT value may be attributable to the unique nano- and microstructures in which γ-Al_2O_3 nanoparticles are dispersed among the grain boundary or in the matrix grain, as revealed by high-resolution transmission electron microscopy. The dispersed γ-Al_2O_3 nanoparticles thus increase phonon scattering sites and reduce thermal conductivity. The results indicated that the nano- and microstructured γ-Al_2O_3/$Bi_{0.4}Sb_{1.6}Te_3$ alloy can serve as a high-performance material for application in TE devices.

Keywords: γ-Al_2O_3/$Bi_{0.4}Sb_{1.6}Te_3$; thermoelectric material; mechanical alloying; nano/microstructure; vacuum hot pressing

1. Introduction

Thermoelectric (TE) materials directly convert thermal energy into electrical energy and *vice versa* and are considered clean energy converters [1]. For practical applications, the conversion efficiency of TE materials is often characterized according to a TE figure of merit, ZT, which is a dimensionless parameter and is conventionally defined as [1]:

$$ZT = (\alpha^2\sigma/\kappa)T \quad (1)$$

where Z, α, σ, κ, and T are figure of merit, Seebeck coefficient, electrical conductivity, thermal conductivity and T absolute temperature, respectively. A high ZT indicates high energy conversion efficiency. Clearly, an efficient TE material with high ZT requires high α, high σ, and low κ. However, satisfying these criteria in a single crystalline bulk material is difficult because these three parameters are interrelated. An increase in α normally implies a decrease in σ (because of carrier density) and an increase in σ implies an increase in the electronic contribution to κ (*i.e.*, the Wiedemann-Franz law); hence, increasing ZT in typical TE materials is extremely difficult. Therefore, materials with ZT higher than that of conventional materials are necessary in industry, and TE conversion efficiency can and must be enhanced by increasing or maintaining the Seebeck coefficient and electrical conductivity and reducing thermal conductivity. However, material classes that contain effective TE properties are rare [2–6].

Over the past 30 years, alloys based on Bi_2Te_3 compounds have been extensively studied and optimized for their use as TE materials. Recently, numerous attempts have been made to increase the ZT of Bi_2Te_3-based TE materials [7–14]. An effective method is to increase the electrical conductivity and reduce the lattice thermal conductivity of TE materials by alloying, doping, or introducing complex crystal structures. Through such approaches, several Bi_2Te_3-based powders, such as CNTs/$Bi_{0.4}Sb_{1.6}Te_3$, C_{60}/$(Bi,Sb)_2Te_3$, BN/$Bi_{0.4}Sb_{1.6}Te_3$, WO_3/$Bi_{0.4}Sb_{1.6}Te_3$, and PbTe/$(Bi,Sb)_2Te_3$ [15–18], with various types of particles were consolidated into bulk shapes by using different consolidation methods. The results indicated that the thermal conductivity of $Bi_{0.4}Sb_{1.6}Te_3$ can be decreased by adding CNTs and C_{60} particles, which eventually increases ZT [15,16]. The thermal conductivity of BN/$Bi_{0.4}Sb_{1.6}Te_3$ and WO_3/$Bi_{0.4}Sb_{1.6}Te_3$ reduces slightly from 1.5 to 1.2 W $m^{-1}K^{-1}$ when the volume fraction of BN and WO_3 is increased from 0 to 7 vol %. However, ZT decreases because adding BN and WO_3 considerably deteriorates the electrical conductivity [17]. Improving ZT of bulk PbTe/$(Bi,Sb)_2Te_3$ samples was unsuccessful because adding PbTe particles drastically reduces the Seebeck coefficient [18]. From the aforementioned results, enhancing ZT clearly strongly depends on the optimal addition of second phase particles to Bi_2Te_3-based alloys.

Recently, Kim *et al.* reported the high ZT value of 1.5 was obtained at 323 K for *p*-type $Bi_{0.5}Sb_{1.5}Te_3$ alloy after doping 0.3 vol % α-Al_2O_3 nanoparticles [19]. Li *et al.* also found that with the introduction of the 1.0 vol % γ-Al_2O_3 particles into *n*-type $Bi_2Se_{0.3}Te_{2.7}$ thermoelectric alloy, $Bi_2Se_{0.3}Te_{2.7}$ exhibits the highest ZT value of 0.99 at about 400 K, being 35% improvement compared to the monolithic $Bi_2Se_{0.3}Te_{2.7}$ alloy [20]. These results indicated the thermoelectric properties of both *p*-type and *n*-type bismuth-antimony-tellurium alloys can be improved with addition of Al_2O_3 particles. However, literature survey indicates the enhancement of *p*-type $Bi_{0.4}Sb_{1.6}Te_3$ alloy with the addition of γ-Al_2O_3 particles has never been reported. Therefore, the γ-Al_2O_3 and $Bi_{0.4}Sb_{1.6}Te_3$ were chosen in present study and the fabrication of γ-Al_2O_3/$Bi_{0.4}Sb_{1.6}Te_3$ composites were performed by mechanical alloying (MA) and vacuum hot pressing. The detailed microstructure and TE properties of samples with varying γ-Al_2O_3 content were investigated. The results showed that the ZT values of the $Bi_{0.4}Sb_{1.6}Te_3$ alloy can be enhanced through the optimal addition of γ-Al_2O_3 particles.

2. Experimental Procedure

$Bi_{0.4}Sb_{1.6}Te_3$ materials with varying contents of γ-Al_2O_3 powder were prepared using a high-energy shaker ball mill installed inside an Ar-purified glove box in which the oxygen and moisture contents in an argon atmosphere were maintained at less than 1 ppm. To prepare Al_2O_3/$Bi_{0.4}Sb_{1.6}Te_3$ powders, a mixture of the elemental metallic powders Bi (99.999%), Sb (99.999%), Te (99.999%), and γ-Al_2O_3 (approximately 99%, with particle size ranging from 0.2 to 7.5 μm with a mean particle size (d(0.5)) of approximately 1.39 μm) was mechanically alloyed using an SPEX 8016 shaker ball mill. The duration of the overall milling process was 2 h. The as-milled γ-Al_2O_3/$Bi_{0.4}Sb_{1.6}Te_3$ composite powders were consolidated in a vacuum hot pressing machine to prepare γ-Al_2O_3/$Bi_{0.4}Sb_{1.6}Te_3$ disks with diameter and thickness of 17 and 10 mm, respectively. Vacuum hot pressing was performed at 573 K under a pressure of 0.7 GPa for 30 min. The

as-milled powders and hot-pressed composite disks were examined using X-ray diffraction (XRD), differential scanning calorimetry, scanning electron microscope (SEM), and transmission electron microscopy (TEM). The TE properties were measured in the direction parallel to the hot-pressed direction. The hot-pressed bulk samples were then cut and polished into 8 × 6 × 6 mm bars. The thermoelectric properties of the hot-pressed samples were investigated using ALTEC-10001 (ITE, Ukraine). This equipment can simultaneously measure the Seebeck coefficient (α), electrical resistivity (σ), and thermal conductivity (κ) of thermoelectric materials from room temperature to 500 °C. The measurement is performed automatically, as well as the analysis of the measurements results, which excludes errors in operators work. ZT was calculated according to Equation (1).

3. Results and Discussion

Figure 1 shows the XRD patterns of the $Bi_{0.4}Sb_{1.6}Te_3$ composite samples with 1 and 3 wt % γ-Al_2O_3 additions after 2 h of milling. The diffraction peaks cited from the database of the $(Bi_{0.2}Sb_{0.8})_2Te_3$ (JCPDS 072-1836) were also plotted with vertical lines in Figure 1 for comparison. All diffraction peak positions and (hkl) values were highly consistent with the standard diffraction data of the pure $(Bi_{0.2}Sb_{0.8})_2Te_3$ phase (JCPDS 072-1836), implying that the $(Bi_{0.2}Sb_{0.8})_2Te_3$ phase can be successfully prepared through high-energy ball milling of γ-Al_2O_3/$Bi_{0.4}Sb_{1.6}Te_3$ composite powders. However, as seen in Figure 1, the Bragg peaks of γ-Al_2O_3 are barely detectable in the XRD patterns of the composite powders of the alloy mixed with γ-Al_2O_3 particles after 2 h of milling, which may be attributable to the low volume fraction of γ-Al_2O_3 particles and their small crystalline size. Similar to the observations regarding the preparation of Al_2O_3/NiAl intermetallic–matrix composite in this study, Lin *et al.* [21] reported that for 5 vol % Al_2O_3 additions in mechanically alloyed NiAl alloys, no Al_2O_3 phase could be detected using XRD after 10 h of milling.

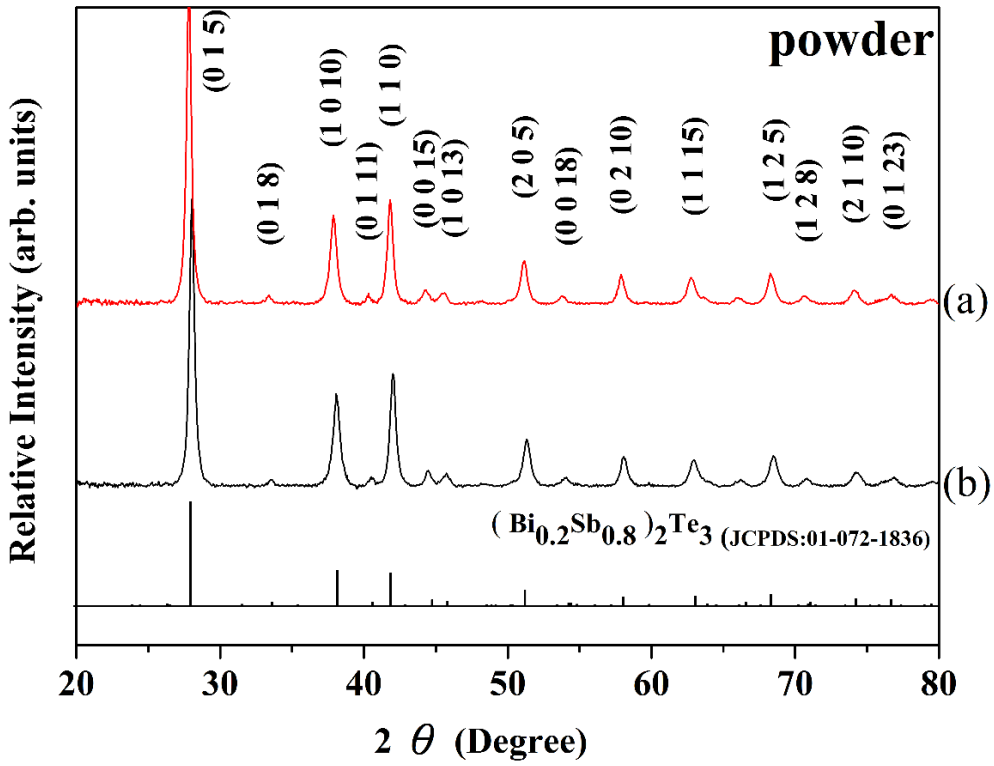

Figure 1. XRD patterns of as-milled $Bi_{0.4}Sb_{1.6}Te_3$ and γ-Al_2O_3-doped $Bi_{0.4}Sb_{1.6}Te_3$ powders. (**a**) 1 wt % Al_2O_3; (**b**) 3 wt % Al_2O_3.

The $Bi_{0.4}Sb_{1.6}Te_3$ composite powders were subsequently consolidated into disks using vacuum hot pressing process; the corresponding XRD patterns are shown in Figure 2. All reflection peaks are attributable to the $(Bi_{0.2}Sb_{0.8})_2Te_3$ phase. Compared with the as-milled composite powders, the peaks of the consolidated samples are narrow because of strain relaxation and grain growth in the $Bi_{0.4}Sb_{1.6}Te_3$ nanograin powders. SEM was used to examine the cross-sectional view of γ-Al_2O_3/$Bi_{0.4}Sb_{1.6}Te_3$ disks after vacuum hot pressing (Figure 3). Although several γ-Al_2O_3 nanoparticles tend to agglomerate each other, most fine γ-Al_2O_3 particles were distributed uniformly within the $Bi_{0.4}Sb_{1.6}Te_3$ matrix. The size distribution ranged from 0.3 μm to less than 50 nm, which is the resolution limit of the microscope. The composition of the particles was determined to be that of pure γ-Al_2O_3 through energy-dispersion X-ray spectrometry analysis. Significant pores were not observed in the cross-sectional view (Figure 3) at 20,000× magnification, indicating that highly dense $Bi_{0.4}Sb_{1.6}Te_3$ bulk samples can be successfully fabricated using vacuum hot pressing. The densities of the $Bi_{0.4}Sb_{1.6}Te_3$ bulk sample measured using the Archimedean method were 6.70 and 6.71 g/cm^3 for 1 and 3 wt % γ-Al_2O_3/$Bi_{0.4}Sb_{1.6}Te_3$ samples, respectively, yielding corresponding relative densities of 93.2% and 93.6%. To observe the microstructure within the γ-Al_2O_3/$Bi_{0.4}Sb_{1.6}Te_3$ composites, $Bi_{0.4}Sb_{1.6}Te_3$ with 1 wt % γ-Al_2O_3 additions (Figure 3) was examined using TEM; a TEM bright-field image is shown in Figure 4. Two types of γ-Al_2O_3 distributions were observed in the composites; most γ-Al_2O_3 nanoparticles smaller than 10 nm in size were homogeneously dispersed along the grain boundary. A small quantity of the γ-Al_2O_3 nanoparticles with irregular shapes and sizes ranging from 60 to 400 nm were embedded within the $Bi_{0.4}Sb_{1.6}Te_3$ matrix. A similar microstructure was reported for the nanocomposites of $CoSb_3$/TiO_2 [13] and ZrNiSn/ZrO_2 [14].

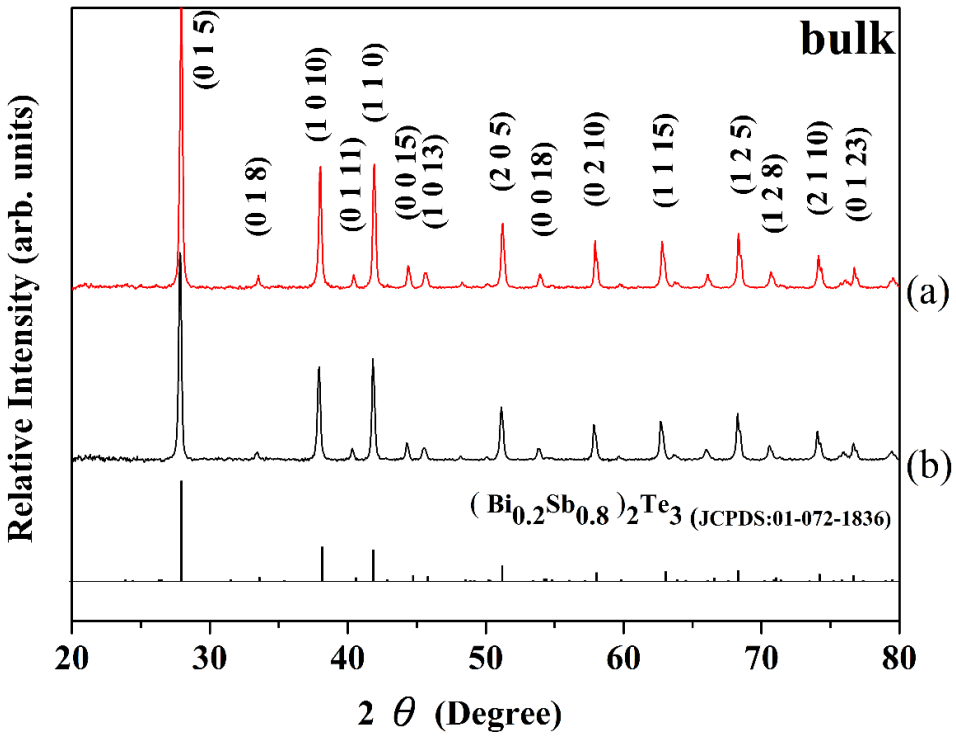

Figure 2. XRD patterns of γ-Al_2O_3-doped $Bi_{0.4}Sb_{1.6}Te_3$ bulk specimens. (**a**) 1 wt % Al_2O_3; (**b**) 3 wt % Al_2O_3.

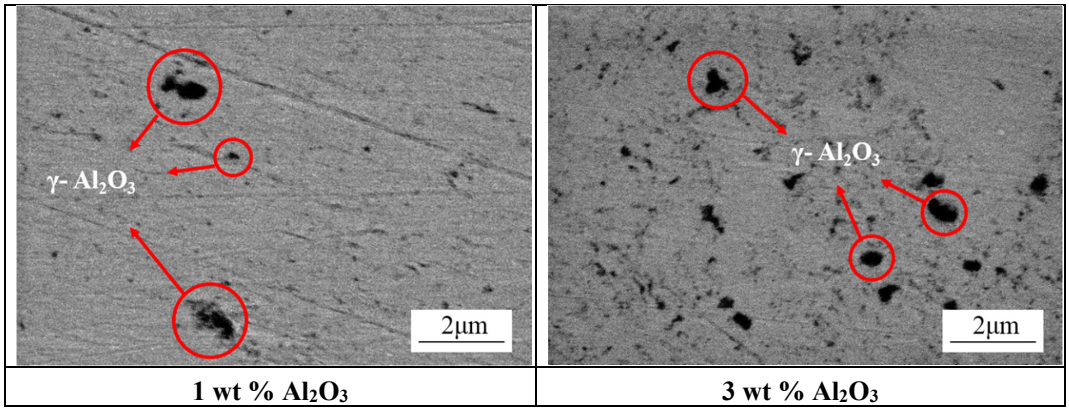

Figure 3. Cross-sectional SEM images of γ-Al_2O_3-doped $Bi_{0.4}Sb_{1.6}Te_3$ disks after vacuum hot pressing at 573 K under a pressure of 0.7 GPa for 30 min (black particles: γ-Al_2O_3).

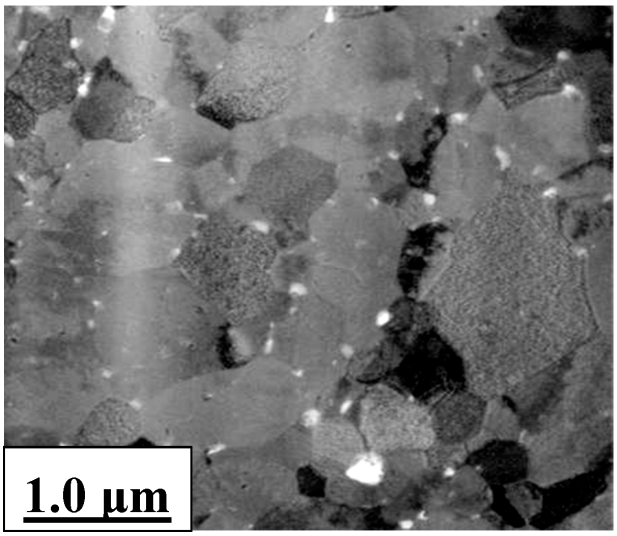

Figure 4. TEM images of the consolidated 1 wt % γ-Al_2O_3/$Bi_{0.4}Sb_{1.6}Te_3$ samples. (white particles: γ-Al_2O_3).

Figure 5 shows the TE properties of the γ-Al_2O_3/$Bi_{0.4}Sb_{1.6}Te_3$ composite samples characterized at temperatures ranging from 298 to 473 K. The Seebeck coefficient variations as a function of temperature are depicted in Figure 5a. All samples had positive Seebeck coefficients, suggesting that they are *p*-type conductive. As shown in Figure 5a, the Seebeck coefficient values of the γ-Al_2O_3/$Bi_{0.4}Sb_{1.6}Te_3$ bulk composite samples decreased with increasing γ-Al_2O_3 content. For most samples, the Seebeck coefficient initially increases rapidly at 300–375 K, which is consistent with the Mott formula [22], but after peaking, it starts decreasing with rising temperatures because of the thermal excitation of extrinsic charge carriers at high temperatures. The maximum value of the Seebeck coefficient is 242, 234 and 229 μV/K at 373 K for 0, 1 and 3 wt % γ-Al_2O_3/$Bi_{0.4}Sb_{1.6}Te_3$ samples, respectively. Figure 5b shows the temperature dependence of electrical conductivity. The samples exhibited a metallic dependence: conductivity gradually decreased as temperature increased from 300 to 473 K. Electrical conductivity of γ-Al_2O_3/$Bi_{0.4}Sb_{1.6}Te_3$ composite decreases as γ-Al_2O_3 particles increases. The highest electrical conductivities at 300 K were observed for 1 and 3 wt % γ-Al_2O_3/$Bi_{0.4}Sb_{1.6}Te_3$ samples, with values of 1080 and 895 Ω^{-1} cm^{-1}, respectively. The power factor (PF) of TE materials is usually calculated as PF = $\alpha^2\sigma$; Figure 5c is a graph of the PF of $Bi_{0.4}Sb_{1.6}Te_3$ bulk composite samples *versus* the temperature. All samples showed positive values in the whole temperature range of measurement, indicating *p*-type semiconducting behavior. The 1 wt %

γ-Al_2O_3/$Bi_{0.4}Sb_{1.6}Te_3$ samples exhibited the highest PF (5.4 $mWm^{-1} \cdot K^{-2}$ at 298 K). The temperature dependence of thermal conductivity is shown in Figure 5d. The 3 wt % γ-Al_2O_3/$Bi_{0.4}Sb_{1.6}Te_3$ samples have significantly lower thermal conductivity than the 1 wt % γ-Al_2O_3/$Bi_{0.4}Sb_{1.6}Te_3$ samples in the whole temperature range. The lowest value of thermal conductivity for this sample was 1.12 W/mK, which was obtained at 373 K.

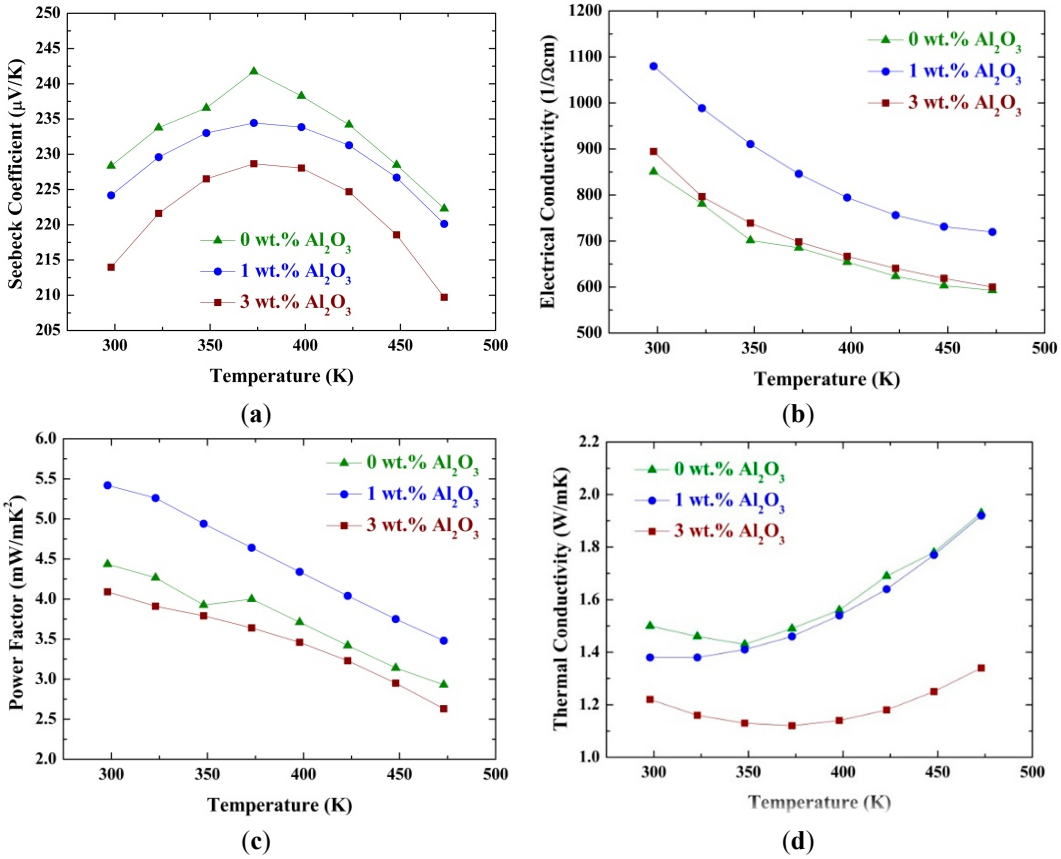

Figure 5. Temperature dependence of the TE properties for the γ-Al_2O_3/$Bi_{0.4}Sb_{1.6}Te_3$ specimens: (**a**) Seebeck coefficient; (**b**) electrical resistivity; (**c**) PF; and (**d**) thermal conductivity.

The variation of ZT as a function of temperature for the γ-Al_2O_3/$Bi_{0.4}Sb_{1.6}Te_3$ bulk specimens is shown in Figure 6.

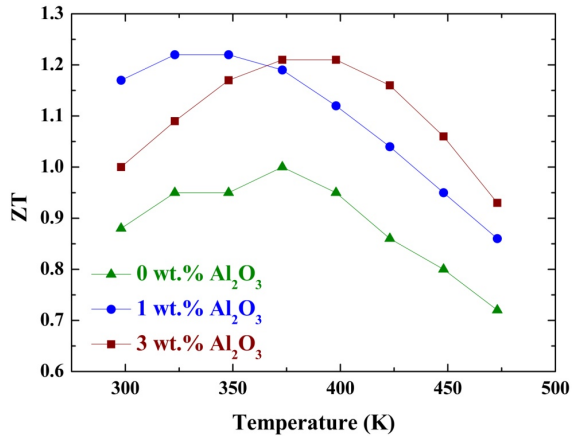

Figure 6. Variation of ZT as a function of temperature for γ-Al_2O_3/$Bi_{0.4}Sb_{1.6}Te_3$ bulk samples.

For the 1 wt % γ-Al_2O_3/$Bi_{0.4}Sb_{1.6}Te_3$ sample, a high ZT value can be obtained within the entire temperature range because of high PFs and low thermal conductivity; ZT at 300 K is 1.17 and increases with increasing temperature, peaking at 1.22 at 323 and 348 K, before subsequently decreasing to 0.86 at 473 K. For the 3 wt % γ-Al_2O_3/$Bi_{0.4}Sb_{1.6}Te_3$ composite sample (Figure 6), ZT at 300 K is 1.0 and increases with increasing temperature, peaking at 1.21 at 373 and 398 K, before subsequently decreasing to 0.93 when the temperature increases to 473 K.

Several studies have reported the preparation of nanocomposite $Bi_{0.4}Sb_{1.6}Te_3$ bulk samples [15–17,22–26] through BM and hot pressing or spark plasma sintering (SPS). TE properties and preparation methods are listed in Table 1. The ZT values of the consolidated $Bi_{0.4}Sb_{1.6}Te_3$ alloys as a function of temperature are plotted in Figure 7, and the results of this study are included for comparison.

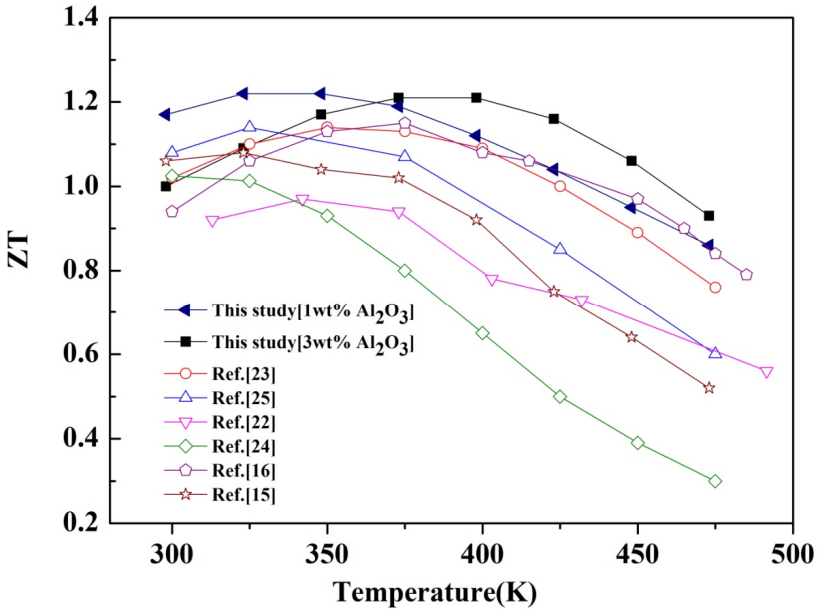

Figure 7. Temperature dependence of ZT of the $Bi_{0.4}Sb_{1.6}Te_3$-based bulk specimens prepared through various methods.

In this study, ZT of the γ-Al_2O_3/$Bi_{0.4}Sb_{1.6}Te_3$ sample at 298–473 K were 0.86–1.22 (1 wt % γ-Al_2O_3) and 0.93–1.21 (3 wt % γ-Al_2O_3), with an average value of 1.10 for both samples. Compared with other studies, the ZT obtained in this study at high temperatures are higher. Advances in ZT can be achieved through considerable reductions in thermal conductivities through phonon scattering. Incorporating nanoparticles into TE materials to act as additional phonon scattering sites inside the grain boundary or matrix regions has recently been demonstrated effectively increase ZT [27–29]. According to this approach, for nano- and microstructured TE composite materials shown in Figure 4, the dispersed γ-Al_2O_3 nanoparticles are expected to create an additional grain boundary and interfacial area, which increases phonon scattering and decreases thermal conductivity. To further verify this argument, the temperature dependence of lattice thermal conductivity (κ_l) and electronic thermal conductivity (κ_e) of present γ-Al_2O_3/$Bi_{0.4}Sb_{1.6}Te_3$ samples are shown in Figure 8. κ_l was calculated by subtracting the electronic thermal conductivity κ_e from κ, and κ_e is calculated by the Wiedemann–Franz relation, $\kappa_e = L\sigma T$ (where $L = 2.0 \times 10^{-8}$ V^2/K^2 is Lorenz number, σ is electrical conductivity, and T is absolute temperature) [30].

Table 1. TE properties and preparation methods of typical $Bi_{0.4}Sb_{1.6}Te_3$-based nanocomposites.

Nanocomposite	Highest ZT	ZT(>400 K)	Method[a,b]	Ref.
$Bi_{0.4}Sb_{1.6}Te_3$	1.15 at 350 K	0.2~0.4	BM + HP (200 MPa/430 C/2 h)	[24]
$Bi_{0.4}Sb_{1.6}Te_3$	1.14 at 323 K	0.2~0.74	BM (300 rpm/10 h) + SPS (50 MPa/420 C/10 min)	[25]
$Bi_{0.4}Sb_{1.6}Te_3$	1.15 at 350 K	0.63~0.9	BM (1200 rpm/5 h) + SPS (60 MPa/420 C/5 min)	[23]
$Bi_{0.4}Sb_{1.6}Te_3$	1.0 at 300 K	-	BM (400 rpm/2 h) + SPS (50 MPa/450 C/5 min)	[26]
$Bi_{0.4}Sb_{1.6}Te_3$ + 4 wt % Te	0.98 at 343 K	0.55~0.68	BM (400 rpm/12 h) + HP (60 MPa/290 C/1 h) + ECAE (753 K)	[22]
$Bi_{0.4}Sb_{1.6}Te_3$ + 1 wt % CNT	1.08 at 323 K	0.52~0.92	ZM + BM + HP (27.6 MPa/440 C/10 min)	[15]
$Bi_{0.4}Sb_{1.6}Te_3$ + 1.5 wt % C_{60}	1.15 at 375 K	0.79~1.08	BM (500~2220 rpm/30 min) + sinter (5 kbar/400 C) +annealing (300 C/2 h)	[16]
$Bi_{0.4}Sb_{1.6}Te_3$ + 7 wt % BN	0.54 at 300 K	-	BM (1200 rpm/5 h) + HP (425 MPa/550 C/30 min)	[17]
$Bi_{0.4}Sb_{1.6}Te_3$ + 7 wt % WO_3	0.75 at 300 K	-	BM (1200 rpm/5 h) + HP (425 MPa/550 C/30 min)	[17]
$Bi_{0.4}Sb_{1.6}Te_3$ + 1 wt % Al_2O_3	1.22 at 340 K	0.86~1.12	BM + HP (700 MPa/300 C/1 h)	This work
$Bi_{0.4}Sb_{1.6}Te_3$ + 3 wt % Al_2O_3	1.21 at 398 K	0.93~1.21	BM + HP (700 MPa/300 C/1 h)	This work

a: BM: ball milling; SPS: spark plasma sintering; ECAE: equal channel angular extrusion; b: Experimental details are listed in parentheses.

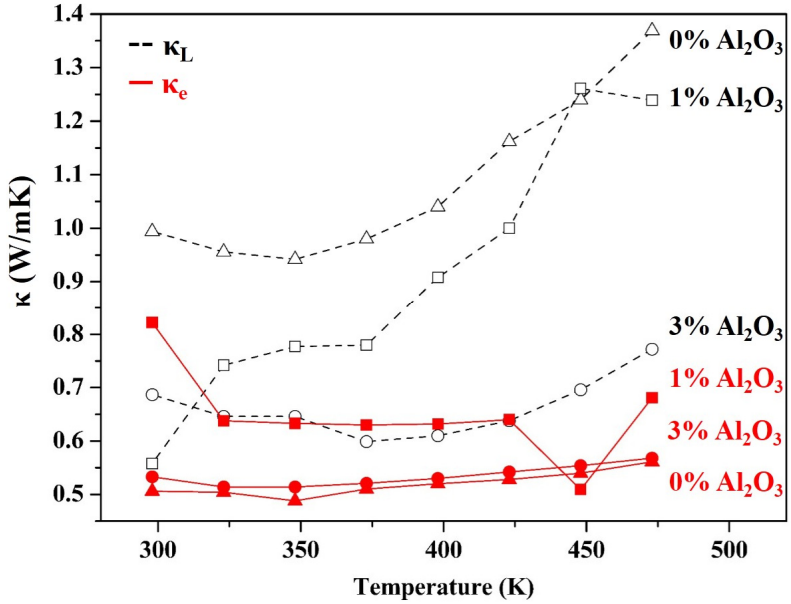

Figure 8. Temperature dependence of lattice thermal conductivity (κ_l) and electronic thermal conductivity (κ_e) for the γ-Al_2O_3/$Bi_{0.4}Sb_{1.6}Te_3$ bulk samples.

Accordingly, the lattice thermal conductivity κ_l decreased with the addition of γ-Al_2O_3 particles, while the electronic thermal conductivity κ_e decreased less drastically than did the lattice thermal conductivity. It is thus concluded that the decrease in thermal conductivity with increasing the amount of γ-Al_2O_3 particles was mainly due to the reduction in lattice thermal conductivity. Bi-Sb-Te alloys are categorized as low-temperature TE materials, and their use at temperatures higher than 400 K is limited because of low TE performance. A satisfactory ZT value at high temperatures is vital for power generation. Because no other Bi-Sb-Te material with a similarly high ZT in this temperature range has been reported, $Bi_{0.4}Sb_{1.6}Te_3$ bulk samples containing γ-Al_2O_3 particles have considerable potential as a high-performance material for application in TE devices in the temperature range 348–473 K.

4. Conclusions

Through MA and vacuum hot pressing, *p*-type γ-Al_2O_3/$Bi_{0.4}Sb_{1.6}Te_3$ composites were fabricated. No significant pores were observed in the hot-pressed samples, indicating that highly dense $Bi_{0.4}Sb_{1.6}Te_3$ bulk samples can be successfully prepared using the proposed approach. The influence of the alumina content on TE properties was measured in the temperature range 300–473 K. The measured Seebeck coefficient, electrical resistivity, and thermal conductivity indicate that adding an optimal amount of γ-Al_2O_3 particles improves the TE performance of the γ-Al_2O_3/$Bi_{0.4}Sb_{1.6}Te_3$ composites. High TE performance with ZT as high as 1.22 and 1.21 were achieved at 373 and 398 K for samples containing 1 and 3 wt % γ-Al_2O_3 particles. These ZT values are higher than those of several reported monolithic $Bi_{0.4}Sb_{1.6}Te_3$ samples prepared through BM and hot pressing or SPS. The achieved high ZT value may be attributable to the unique nano- and microstructures in which γ-Al_2O_3 nanoparticles were dispersed along the grain boundary or inside the matrix grain, as revealed through high-resolution TEM. The dispersed γ-Al_2O_3 nanoparticles thus increase phonon scattering sites and reduce thermal conductivity. The ZT values of these samples at 298–423 K are 1.0–1.22. Such ZT characteristics render γ-Al_2O_3/$Bi_{0.4}Sb_{1.6}Te_3$ suitable for power generation applications because other materials with similarly high ZT are yet to be reported in this temperature range.

Acknowledgments: The authors are grateful for the financial support of this study by the Ministry of Science and Technology of the Taiwan (ROC) under Grant No. MOST 103-2221-E-019-013.

Author Contributions: Chung-kwei Lin and May-Show Chen carried out the sample preparation and data analysis work. Rong-Tan Huang conducted the SEM and TEM study. The measurement of thermoelectric properties was performed by Yu-Chun Cheng. Pee-Yew Lee designs the experimental procedure and prepared the manuscript of the paper.

Conflicts of Interest: The authors declare no conflict of interest.

References

1. Tritt, T.M.; Subramanian, M.A. Thermoelectric Materials, Phenomena, and Applications: A bird's eye view. *MRS Bull.* **2006**, *31*, 188–198. [CrossRef]
2. Tang, X.; Xie, W.; Li, H.; Du, B.; Zhang, Q.; Tritt, T.M.; Uher, C. High-performance nanostructured thermoelectric materials prepared by melt spinning and spark plasma sintering. In *Thermoelectrics and Its Energy Harvesting: Materials Preparation, and Characterization in Thermoelectrics*; Rowe, D.M., Ed.; CRC Taylor and Francis: Boca Raton, FL, USA, 2012; pp. 16.1–16.33.
3. DiSalvo, F.J. Thermoelectric cooling and power generation. *Science* **1999**, *285*, 703–706. [CrossRef] [PubMed]
4. Kim, W.; Zide, J.; Gossard, A.; Klenov, D.; Stemmer, S.; Shakouri, A.; Majumdar, A. Thermal conductivity reduction and thermoelectric figure of merit increase by embedding nanoparticles in crystalline semiconductors. *Phys. Rev. Lett.* **2006**, *96*, 045901-1–045901-4. [CrossRef] [PubMed]
5. Dmitriev, A.V.; Zvyagin, I.P. Current trends in the physics of thermoelectric materials. *Phys. Usp.* **2010**, *53*, 789–803. [CrossRef]
6. Minnich, A.J.; Dresselhaus, M.S.; Ren, Z.F.; Chen, G. Bulk nanostructured thermoelectric materials: Current research and future prospects. *Energy Environ. Sci.* **2009**, *2*, 466–479. [CrossRef]
7. Ballikaya, S.; Uzar, N.; Yildirim, H.; Chi, H.; Su, X.; Tan, G.; Tang, X.; Uher, C. Lower thermal conductivity and higher thermoelectric performance of Fe-substituted and Ce, Yb double-filled p-type skutterudites. *J. Electron. Mater.* **2013**, *42*, 1622–1627. [CrossRef]
8. Kadhim, A.; Hmood, A.; Hassan, H.A. Preparation of $Bi_{0.4}Sb_{1.6}Se_{3x}Te_{3(1-x)}$ hexagonal rods and effect of Se on structure and electrical property. *Solid State Sci.* **2013**, *21*, 110–115. [CrossRef]
9. Buga, S.G.; Serebryanaya, N.R.; Dubitskiy, G.A.; Semenova, E.E.; Aksenenkov, V.V.; Blank, V.D. Structure and electrical properties of Sb_2Te_3 and $Bi_{0.4}Sb_{1.6}Te_3$ metastable phases obtained by HPHT treatment. *High Press. Res. Int. J.* **2011**, *31*, 86–90. [CrossRef]
10. Zhang, Q.; Znang, Q.; Chen, S.; Liu, W.; Lukas, K.; Yan, X.; Wang, H.; Wang, D.; Opeil, C.; Chen, G.; *et al*. Suppression of grain growth by additive in nanostructured p-type bismuth antimony tellurides. *Nano Energy* **2012**, *1*, 183–189. [CrossRef]
11. Xie, W.; Wang, S.; Zhu, S.; Ho, J.; Tang, X.; Zhang, Q.; Tritt, T.M. High performance Bi_2Te_3 nanocomposites prepared by single-element-melt-spinning spark-plasma sintering. *J. Mater. Sci.* **2013**, *48*, 2745–2760. [CrossRef]
12. Pichanusakorn, P.; Bandaru, P. Nanostructured thermoelectrics. *Mater. Sci. Eng. R.* **2010**, *67*, 19–63. [CrossRef]
13. Medlin, D.L.; Snyder, G.J. Interfaces in bulk thermoelectric materials: A review for Current Opinion in Colloid and Interface Science. *Curr. Opin. Colloid In.* **2009**, *14*, 226–235. [CrossRef]
14. Chen, L.D.; Huang, X.Y.; Zhou, M.; Shi, X.; Zhang, W.B. The high temperature thermoelectric performances of $Zr_{0.5}Hf_{0.5}Ni_{0.8}Pd_{0.2}Sn_{0.99}Sb_{0.01}$ alloy with nanophase inclusions. *J. Appl. Phys.* **2006**, *99*, 064305-1–064305-6. [CrossRef]
15. Ren, F.; Wang, H.; Mechhofer, P.A.; Kiggans, J.O. Thermoelectric and mechanical properties of muti-walled carbon nanotube doped $Bi_{0.4}Sb_{1.6}Te_3$ thermoelectric material. *Appl. Phys. Lett.* **2013**, *103*, 221907-1–221907-5. [CrossRef]
16. Popov, M.; Buga, S.; Vysikaylo, P.; Stepanov, P.; Skok, V.; Medvedev, V.; Tatyanin, F.; Denisov, V.; Kirichenko, A.; Aksenenkov, V.; *et al*. C_{60}-doping of nanostructured Bi-Sb-Te thermoelectrics. *Phys. Status Solidi A* **2011**, *208*, 2783–2789. [CrossRef]
17. Lee, J.S.; Oh, T.S.; Hyun, D.B. Thermoelectric properties of the hot-press $(Bi_{0.2}Sb_{0.8})_2Te_3$ alloy with addition of BN and WO_3 powders. *J. Mater. Sci.* **2000**, *35*, 881–887. [CrossRef]

18. Ganguly, S.; Zhou, C.; Morelli, D.; Sakamoto, J.; Uher, C.; Brock, L.S. Synthesis and evaluation of lead telluride/bismuth antimony telluride nanocomposites for thermoelectric applications. *J. Solid State Chem.* **2011**, *184*, 3195–3201. [CrossRef]
19. Kim, K.T.; Ha, G.H. Fabrication and ehanced thermoelectric properties of alumina nanoparticles-dispersed $Bi_{0.5}Sb_{1.5}Te_3$ Matrix Composites. *J. Nanomater.* **2013**, *2013*, 1–6.
20. Fei, L.; Huang, X.Y.; Sun, Z.L.; Ding, J.; Jiang, J.; Jiang, W.; Chen, L.D. Enhanced thermoelectric properties of *n*-type Bi_2Te_3-based nanocomposite fabricated by spark plasma sintering. *J. Alloy. Compd.* **2011**, *509*, 4769–4773.
21. Lin, C.K.; Hong, S.S.; Lee, P.Y. Formation of NiAl-Al_2O_3 intermetallic-matrix composite powders by mechanical alloying technique. *Intermetallics* **2000**, *8*, 1043–1048. [CrossRef]
22. Fan, X.A.; Yang, J.Y.; Zhu, W.; Bao, S.Q.; Duan, X.K.; Xiao, C.J.; Li, K. Preferential orientation and thermoelectric properties of p-type $Bi_{0.4}Sb_{1.6}Te_3$ system alloys by mechanical alloying and equal channel angular extrusion. *J. Alloy. Compd.* **2008**, *461*, 9–13. [CrossRef]
23. Jiang, J.; Chen, L.; Bai, S.; Yao, Q. Thermoelectric performance of p-type Bi-Sb-Te materials prepared by spark plasma sintering. *J. Alloy. Compd.* **2005**, *390*, 208–211. [CrossRef]
24. Li, Y.L.; Jiang, J.; Xu, G.J.; Li, W.; Zhou, L.M.; Li, Y.; Cui, P. Synthesis of micro/nanostructured p-type $Bi_{0.4}Sb_{1.6}Te_3$ and its thermoelectrical properties. *J. Alloy. Compd.* **2009**, *480*, 954–957. [CrossRef]
25. Son, J.H.; Oh, M.W.; Kim, B.S.; Park, S.D.; Min, B.K.; Kim, M.H.; Lee, H.W. Effect of ball milling time on the thermoelectric properties of p-type $(Bi,Sb)_2Te_3$. *J. Alloy. Compd.* **2013**, *566*, 168–174. [CrossRef]
26. Osvenskiy, V.B.; Panchenko, V.P.; Parkhomenko, Y.N.; Sorokin, A.I.; Bogomolov, D.I.; Bublik, V.T.; Tabachkova, N.Y. Nonmonotonic change in the structural grain size of the $Bi_{0.4}Sb_{1.6}Te_3$ hermoelectric material synthesised by spark plasma sintering. *J. Alloy. Compd.* **2014**, *586*, S413–S418. [CrossRef]
27. Harman, T.C.; Taylor, P.J.; Walsh, M.P.; LaForge, B.E. Quantum dot superlattice thermoelectric materials and devices. *Science* **2002**, *27*, 2229–2232. [CrossRef] [PubMed]
28. Zhou, M.; Li, J.F.; Kita, T. Nanostructured $AgPb_mSbTe_{m+2}$ system bulk materials with enhanced thermoelectric performance. *J. Am. Chem. Soc.* **2008**, *130*, 4527–4532. [CrossRef] [PubMed]
29. He, J.; Gueguen, A.; Sootsman, J.R.; Zheng, J.C.; Wu, L.; Zhu, Y.; Kanatzidis, M.G.; Dravid, V.P. Role of self-organization, nanostructuring, and lattice strain on phonon transport in $NaPb_{18-x}Sn_xBiTe_{20}$ thermoelectric materials. *J. Am. Chem. Soc.* **2009**, *131*, 17828–17835. [CrossRef] [PubMed]
30. Goldsmith, H.J.; Douglas, R.W. The use of semiconductors in thermoelectric refrigeration. *Br. J. Appl. Phys.* **1954**, *5*, 386–390. [CrossRef]